IEEE Access
Multidisciplinary | Rapid Review | Open Access Journal

Received July 17, 2019, accepted July 26, 2019, date of publication July 30, 2019, date of current version August 15, 2019.

Digital Object Identifier 10.1109/ACCESS.2019.2932123

Grating Lobe Suppression of Non-Uniform Arrays Based on Position Gradient and Sigmoid Function

XIAOMIN XU[1], CHENG LIAO[1], LIANG ZHOU[1,2], AND FAN PENG[1]
[1]Institute of Electromagnetics, Southwest Jiaotong University, Chengdu 610031, China
[2]724 Research Institute, China Shipbuilding Industry Corporation, Nanjing 210003, China

Corresponding author: Cheng Liao (c.liao@swjtu.edu.cn)

This work was supported by the National Natural Science Foundation of China under Grant 61771407.

ABSTRACT A super-multivariate optimization algorithm is proposed to suppress the grating lobes (GLs) of non-uniform arrays. For position-only variable cases of any huge array, it is always difficult to deal with by using clustering algorithm because of thousands of variables. The proposed method achieves grating lobe suppression (GLS) by taking position gradient of dynamic maximum GL and obtaining phase difference by comparing with every element, which requires only precious few extra computations. When gradient function varying with each element position is established, an appropriate sigmoid function will be introduced and used to control the magnitude of small element displacement. After each generation of element-movement operation, electric field of all elements are superimposed and partially cancelled out each other in the target direction. In addition, the gradient computing does not significantly increase the cost of total computation under multi-variable conditions, which avoids the unacceptable cost of conventional clustering optimization algorithm. In this paper, a 16×16-element array is optimized, and a result comparison with random optimization (RO), particle swarm optimization (PSO), and gradient algorithm (GA) is present. The validity of the proposed algorithm for GLS is verified through using a 100×100-element array. In the final, a large array antenna based on subarrays is optimized for a low sidelobe level (SLL) below -20dB using the proposed algorithm. The results meet the requirements and show the effectiveness of the proposed algorithm.

INDEX TERMS Grating lobe suppression, gradient, large non-uniform arrays, optimization algorithm, sigmoid function.

I. INTRODUCTION

Phased array (PA) antennas, due to their good radiation performance and excellent control over the radiating beam, have been widely used in various applications [1]–[5]. For deep space observation, target detection and medical imaging cases, low grating lobe level (GLL) is required as a design goal, which means that the GLS becomes a major concern during the design of the PA. However, this could become a big challenge for improving the radiation performance, especially when the arrays contain antenna elements with electrically large aperture size. The reason lies in that the large spacing easily leads to grating lobes, even when the beam of the array is not scanning. Therefore, the suppression of GLs of PAs with large spacing between elements needs to be studied.

The associate editor coordinating the review of this manuscript and approving it for publication was Mingchun Tang.

In order to suppress the GLs of PA, the influence factors, such as the amplitudes or phases of the elements, the layouts of the array, the element rotation angle or even using a good performance element antenna, could be considered as the variables to optimize the overall performance [6], [7]. The grating lobe suppression problem we discuss here is about the array antennas with only the element position as variables. Thus, many numeral algorithms are employed into the optimization process to solve the GLS problems, such as particle swarm optimization (PSO) [8], [9], genetic algorithm (GA) [10], least square method [11], [12] and other methods [13]–[16]. However, a problem for them is that they are not suitable for optimizing the radiation patterns of huge arrays with likely more than 10-thousand elements. When the number of variables is overlarge, those algorithms often require a lot of computational costs. Besides, it is difficult for them to ensure the convergence of cost function and thus to obtain effective optimization results. The iterative fast Fourier

transform (iFFT) is an efficient synthesis algorithm of huge arrays [12], [17]. But it can only be used to deal with uniform problems, at least not directly with non-uniform problems. In addition, the convex optimizations (CO) [18], [19] or the gradient methods [20], [21] are often used to process the multivariable and non-uniform problems.

In this letter, we propose a method based on the gradient and sigmoid function so as to consider the GLS problem of non-uniform huge arrays with large element spacing in position-only cases. In this method, positions of all elements will be adjusted to trim their spatial phases for decreasing the highest GL in each iteration. Meanwhile, the introduced sigmoid function is used to define different small displacement of elements, which can enhance the convergence of the proposed algorithm. The principle of proposed algorithm and details of sigmoid function control are elaborated in section II. Then section III presents some examples of small and large arrays. Some analysis is given in section IV.

II. PRINCIPLE AND FLOW OF THE ALGORITHM

A. PRINCIPLE OF THE ALGORITHM

The proposed algorithm suppresses the grating lobe level by translating elements. Thus, the significant procedure is to establish the relationship between the maximum GLL and the position shift of each element. The gradient function is an effective link for the two variables.

The array factor (AF) of a planar array with $M \times N$ element antennas can be calculated by using (1).

$$E = \sum_{i=1}^{M \times N} I_i e^{jk(x_i u + y_i v)} \tag{1}$$

where $k = 2\pi/\lambda$ is the wave number in free space, λ is the operating wavelength. I_i is the excitation of the element (i ranges from 1 to $M \times N$), and the coefficients of direction are set as $u = \sin(\theta)\cos(\varphi)$ and $v = \sin(\theta)\sin(\varphi)$. This study focuses on the position-only problems that all elements are fed with the same excitation $I_i = I_0 e^{j\gamma_0}$, where I_0 and γ_0 are the amplitude and initial phase of the excitation I_i, respectively. Both I_0 and γ_0 are constants. The x_i and y_i represent coordinate positions of the i-th element.

According to (1), the position gradient of the pattern of the i-th element can be written as

$$\nabla E = \boldsymbol{e}_x \frac{\partial E}{\partial x_i} + \boldsymbol{e}_y \frac{\partial E}{\partial y_i} \tag{2}$$

where

$$\begin{cases} \dfrac{\partial E}{\partial x_i} = jkuI_i e^{jk(x_i u + y_i v)} = A_{ix} e^{j\varphi_i} \\ \dfrac{\partial E}{\partial y_i} = jkvI_i e^{jk(x_i u + y_i v)} = A_{iy} e^{j\varphi_i} \end{cases} \tag{3}$$

where $A_{ix} = jkuI_i$, $A_{iy} = jkvI_i$, and $\varphi_i = x_i u + y_i v$. Taking $\partial E/\partial x$ as an example, it represents the relationship between the array's pattern and the x-axis position shift of each element. When an element moves to the positive direction of the x-axis, the pattern can produce an increment, which can be denoted as

$$\Delta E = \frac{\partial E}{\partial x_i} \cdot \Delta x_i = A_{ix} e^{j(\varphi_i + \Delta\varphi_{xi})} \cdot \Delta x_i \tag{4}$$

where Δx_i represents the tiny position shift of i-th element, $\Delta\varphi_{xi} = ku\Delta x_i$ represents the phase increment of the term of $\partial E/\partial x$. As for the y-axis, there is a same form of function like (4), and $\Delta\varphi_{yi} = kv\Delta y_i$.

The direction of the maximum GL is marked as (u_m,v_m), so the AF of (u_m,v_m) can be represent as $E(u_m,v_m) = A_m e^{j\varphi 0}$, where A_m is the amplitude and φ_0 is the phase. The phase difference between the $E(u_m,v_m)$ and the AF increment of the i-th element, $\Delta E_i(u_m,v_m)$, can be written as

$$\Delta p_i = \varphi_0 - (\varphi_i + \Delta\varphi_i) \tag{5}$$

where Δp_i is normalized into the interval of [-π, π]. According to the principle of vector coherent superposition, the increment along with x-axis can also be represented as

$$\Delta E_i(u_m, v_m) = |\Delta E_i(u_m, v_m)| \cdot \cos(\Delta p_i) \tag{6}$$

Then, three cases need to be discussed:

1) $|\Delta p_i| < \pi/2$, it means that both of $E(u_m,v_m)$ and $\Delta E_i(u_m,v_m)$ are positive or negative. When the element moves to positive side, $E(u_m,v_m)$ increases, so the element i should be moved to the negative side to generate an opposite phase to decrease the $E(u_m,v_m)$.
2) $|\Delta p_i| > \pi/2$, it means that $E(u_m,v_m)$ and $\Delta E_i(u_m,v_m)$ have the phases with opposite sign. When the element moves to the positive side, $E(u_m,v_m)$ decreases, so the strategy of this case is moving the element i to positive side.
3) $|\Delta p_i| = \pi/2$, it means that $E(u_m,v_m)$ and $\Delta E_i(u_m,v_m)$ are orthogonal to each other, and the tiny movement of the element do not contribute to the AF in this case. Therefore, there is no need to move that element.

After discussing the three situations of the phase difference, all the element has its own suitable strategy of shifting. By the way, the process of data in y-axis is the same as that in x-axis discussed above.

B. SIGMOID FUNCTION

In this subsection we discuss how to control the position shift of each element. Before that, a displacement matrix of the j-th iteration, marked as $\boldsymbol{D}^{(j)}$, is denoted at first. It can be expressed as

$$\boldsymbol{D}^{(j)} = \begin{bmatrix} D_{11}^{(j)} & D_{12}^{(j)} & \cdots & D_{1N}^{(j)} \\ D_{21}^{(j)} & D_{22}^{(j)} & \cdots & D_{2N}^{(j)} \\ \vdots & \vdots & \ddots & \vdots \\ D_{M1}^{(j)} & D_{M1}^{(j)} & \cdots & D_{MN}^{(j)} \end{bmatrix} \tag{7}$$

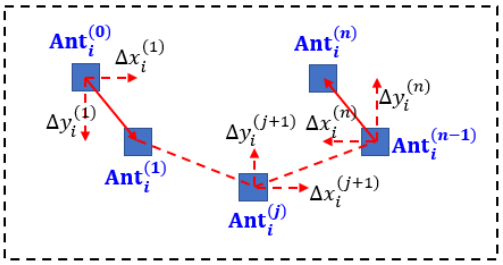

FIGURE 1. Position of antenna i changes with the iteration steps. The superscript j is the iteration step, and $\Delta x_{i(j)}$, $\Delta y_{i(j)}$ represent the displacement of antenna i during j-th iteration.

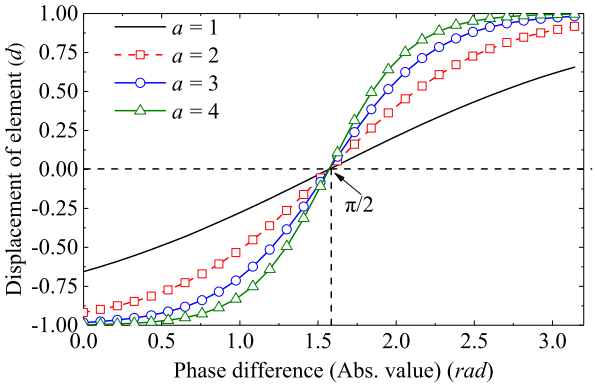

FIGURE 2. Sigmoid function curves indicate the relationship between the absolute value of phase difference and the position shifts of elements at d = 1λ (unit of d is λ, the reference point of curves is set in (π/2,0)).

or separated by two axes, as (8):

$$\begin{cases} \boldsymbol{D}_x^{(j)} = \begin{bmatrix} \Delta x_{11}^{(j)} & \Delta x_{12}^{(j)} & \cdots & \Delta x_{1N}^{(j)} \\ \Delta x_{21}^{(j)} & \Delta x_{22}^{(j)} & \cdots & \Delta x_{2N}^{(j)} \\ \vdots & \vdots & \ddots & \vdots \\ \Delta x_{M1}^{(j)} & \Delta x_{M1}^{(j)} & \cdots & \Delta x_{MN}^{(j)} \end{bmatrix} \\ \boldsymbol{D}_y^{(j)} = \begin{bmatrix} \Delta y_{11}^{(j)} & \Delta y_{12}^{(j)} & \cdots & \Delta y_{1N}^{(j)} \\ \Delta y_{21}^{(j)} & \Delta y_{22}^{(j)} & \cdots & \Delta y_{2N}^{(j)} \\ \vdots & \vdots & \ddots & \vdots \\ \Delta y_{M1}^{(j)} & \Delta y_{M1}^{(j)} & \cdots & \Delta y_{MN}^{(j)} \end{bmatrix} \end{cases} \tag{8}$$

where j is the number of the current iteration, from 1 to n. The subscripts, M and N, represent the number of elements in x-axis and y-axis, respectively. Each $D_{mn(j)}$ the matrix $\boldsymbol{D}^{(j)}$ can be written as $D_{i(j)} = (\Delta x_{i(j)}, \Delta y_{i(j)})$, which means the position shift of antenna i in the j-th iteration, as shown in Fig. 1. Therefore, the displacement matrix $\boldsymbol{D}^{(j)}$ indicates all the position shifts of all the antennas of a M-element array in the current iteration.

In order to control the displacements of each element, the sigmoid function is employed into this problem. The sigmoid function is often used to control the neural network algorithm [22], or the imaging algorithm [23]. Here it is used to make the transformation from the phase difference to the suitable position displacement of element more effective and reasonable. The sigmoid function is given by

$$f_{\text{sigmoid}}(x) = d\left(\frac{2}{1 + e^{-a(|x| - \pi/2)}} - 1\right) \tag{9}$$

where the input x represents the phase difference $|\Delta p_i|$ in our algorithm. Magnitude d is the max value of $|f(x)|$ and we denote it as the upper displacement limit (UDL) of arbitrary element with a unit of 1λ. Coefficient a of (9) represents a tunable factor without unit (referred to as factor a in the following), which can be used to adjust the change intensity from x to $f(x)$, as shown in Fig. 2. The position shifts of $\Delta x^{(j)}$ and $\Delta y^{(j)}$ in (8) are obtained by using (9) and their upper limit are set to d, i.e. the UDL.

Here we discuss the effects of variables in sigmoid. When $d = 1$, the $f(x)$ curves with different factor a are shown in the Fig. 2. The phase differences Δp_i are restricted to the range from 0 to π by taking the absolute value of all the negative phase difference, so that the corresponding position shift can be restricted to the range of $\pm d$. When $0 < |\Delta p_i| < \pi/2$, the element's displacement is negative, and when $\pi/2 < |\Delta p_i| < \pi$, the element's displacement is positive, and $|\Delta p_i| = \pi/2$ is related to zero displacement. These mean the curve of sigmoid function we construct is satisfied the three cases discussed in the last subsection. Thus, the GL should be suppressed after iterations.

Here are some additional explanations. Since the position shift corresponding to $\pm\pi/2$ is 0, all the elements are divided into two groups in which the phase differences of the elements tend to $\pm\pi/2$ as optimization steps increases. And the phase difference between the two groups of elements is about π, which satisfies the inverse phase condition. In this way, the AF now has another representation as

$$|E_m| = \left| I_0 e^{j\gamma_0} \left(\sum_{p \in S} e^{j\varphi_{mp}} + \sum_{q \in \bar{S}} e^{j\varphi_{mq}} \right) \right| \tag{10}$$

where $p = 1, 2, \ldots, P, q = 1, 2, \ldots, Q$, and $P+Q = M \times N$. S is a set contains all the elements with $|\Delta p_i|$ tending to $\pi/2$, $\bar{S}$ is a set contains all the elements with $|\Delta p_i|$ tending to -$\pi/2$, thus, the two groups have a phase difference of π. All the elements have the same amplitude of feed. Then, according to (10), $|E_m|$ will decrease when the difference of the representation $|P-Q|$ approaches zero. Because, if the values of P and Q are quite similar, the elements, both in the two groups, can cancel out the increment of E_m, i.e. $\Delta E(u_m, v_m)$, which is due to the sum of the reverse components of electric fields with opposite phases. Otherwise, if P is obviously greater than Q, or vice versa, most of the elements enhance the E_m because their phases determine that the codirectional components are accumulated. In conclusion, the uniform and dispersed phase distribution, which can lead to a uniform distribution of elements to the two groups, is beneficial to the optimization results. Therefore, the initial position of the array is added with a random displacement matrix, so that the phase difference of

all elements can be more evenly distributed. This strategy can also avoid that the same row (or same column) elements in a rectangular grid array always have the same position shifts.

C. FITNESS FUNCTION

The fitness function we constructed is maximum GL of the current array. It is a dynamic variable because its position changes with iteration. The cost function can be described as

$$Fitness = E_m^{(j)} = \sum_{i=1}^{M\times N} I_i e^{jk\left(x_i^{(j)} u_{im}^{(j)} + y_i^{(j)} v_m^{(j)}\right)} \tag{11}$$

where $E_m^{(j)}$ is denoted as the direction of maximum GL in j-th iteration and also marked as $E(u_{m(j)},v_{m(j)})$ as before.

As well known that the direction of the greatest GL varies with the iteration step j. Thus, we need to determine the distribution region (D-region) of the GLs. The D-region in this work is set to be the whole visible region except the pan mainlobe region which contains the mainlobe and several sidelobes nearest to the mainlobe. Because the sidelobes nearest to the mainlobe are difficult to optimize by means of finite displacement. If the D-region is determined, the direction $(u_{m(j)}, v_{m(j)})$ can be easily identified and the corresponding $E_{m(j)}$ can be extracted from the complete AF matrix by the $u_{m(j)}$ and $v_m^{(j)}$ coordinates. Then, the fitness is obtained. In addition, the complete AF, the direction (u_m, v_m) and the fitness value E_m need to be updated in every iteration.

D. ALGORITHM FLOW

The basic steps of the dynamic algorithm of GLS based on the position gradient are listed as follows:

1) Initialization: Define an original layout of the array, for example, a rectangular grid layout plus a random displacement matrix which is conducive to carry out the optimization. The variables of sigmoid function need to be initialized.
2) AF Calculation: Calculate the AF of the total array, E, then determine the direction of the maximum GL, marked as (u_m, v_m), and extract its electric field E_m.
3) Position gradient: According to (2) and (3), we calculate the position gradient of every element pointing at (u_m, v_m), and get the phase difference, Δp_i (including Δp_{xi} and Δp_{yi}).
4) Sigmoid control: Use the sigmoid function to control the conversion from the phase difference Δp_i to the position shifts, Δx_i and Δy_i, and then generate the displacement matrix $\boldsymbol{D}$, denoted as (7).
5) Overlap detection: Conduct overlap pre-detection of the new layout. If the element i is overlap with neighbor elements, it should be reset to its position obtained from last iteration by adjusting Δx_i or Δy_i or both of two to 0. The detection is repeated until no overlap occurs. After that, the matrix $\boldsymbol{D}$ should be updated to a new matrix $\boldsymbol{D_s}$ with some elements of zero position shifts. The matrix $\boldsymbol{D_s}$ ensure that there is no overlap in the new layout.

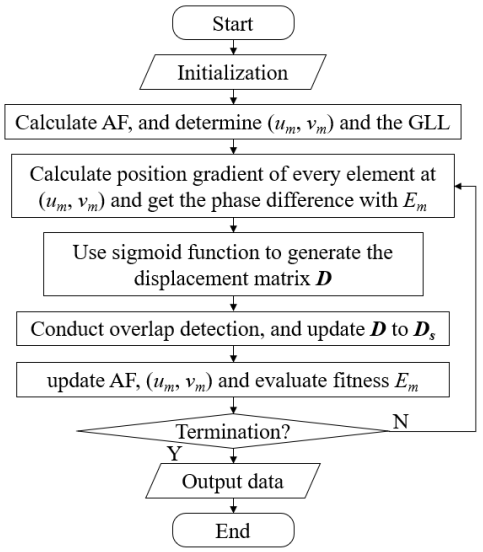

FIGURE 3. Flow chart of the proposed algorithm.

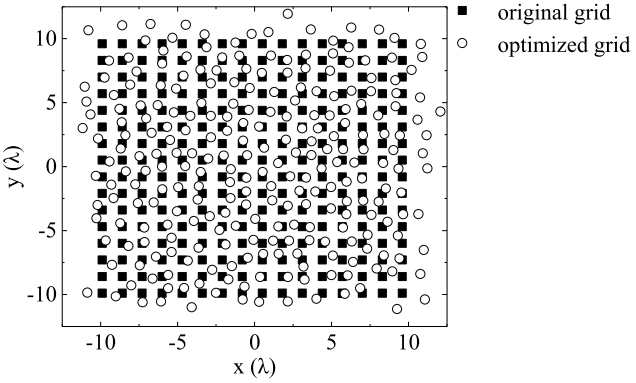

FIGURE 4. Comparison of array layout of 16×16 elements before and after optimization.

6) Fitness evaluation: Recalculate E after loading $\boldsymbol{D_s}$, and update the data of (u_m, v_m), then, evaluate the fitness function of (11), i.e. E_m.
7) Loop and termination: Repeat the steps (3) to (6) until the optimization goal is reached or the iteration arrives at its maximum step.

The flow chart of the proposed algorithm is given in Fig. 3.

III. PARAMETRIC STUDIES AND RESULTS ANALYSIS

A. PARAMETRIC STUDIES OF SIGMOID FUNCTION

In order to further understand the role of the sigmoid function, some comparisons and parametric studies are carried out. A 16×16 elements non-uniform array is taken as an example. The layout of the array is initialized by randomly shifting a rectangular grid array, as shown in Fig. 4. Since the aperture of the element is 1λ× 1λ, the element spacing of the reference rectangular layout is selected as 1.3λ on both the X and Y axes. Thus, there is an enough translation space for the neighboring elements to avoid overlaps.

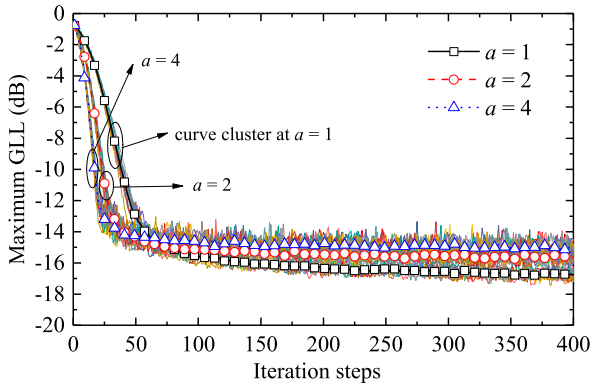

FIGURE 5. Convergence profiles with different factor a in case of 16×16-element antenna array at $d = 0.1\lambda$. Each no symbol mark curve represents once calculation (the same in other figures), and each curve with symbol mark is the average line of each curve cluster with different value a.

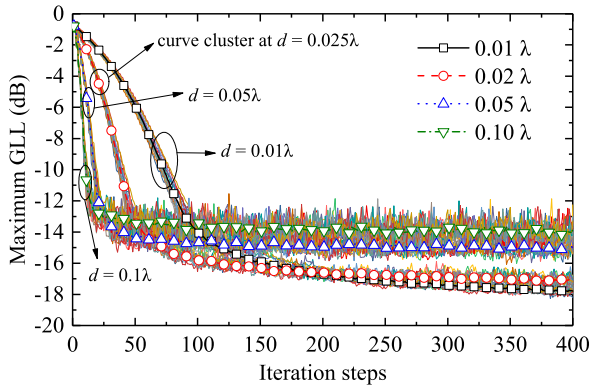

FIGURE 6. Convergence profiles with different UDL d in case of 16×16-element antenna array at $a = 4$. Each curve with symbol mark is the average of its curve cluster with different value d.

Firstly, the influence of the factor a on the convergence curves is investigated and shown in Fig. 5. The d is fixed as 0.1λ and the factor a varies from 1 to 4. It can be found that the rate of convergence becomes faster when the factor a increases in a certain range. When the factor a is greater than 4, the rapidly decreasing portion of convergence curve moves slightly to the left, which means the convergence rate will not increase indefinitely. However, for the later iteration steps, the smaller factor a leads to a better result. The curve with a bigger a and a faster decline rate in the early iteration steps can only converge to a relatively worse value. Because the larger the factor a, the greater the fluctuations of the convergence curve, which will appear and last to the end of the iterations and make the optimization difficult to get finer results.

On the other hand, Fig. 6 plots several curves with varying d and fixed a. An obvious observation is the larger d corresponds to the faster convergence in the early stage and the relatively worse result in the end; Conversely, the smaller d results in the slower convergence in the early stage and the better result in the end. This observation is consistent with the effect of factor a. As a result, we can control the convergence process by changing d only.

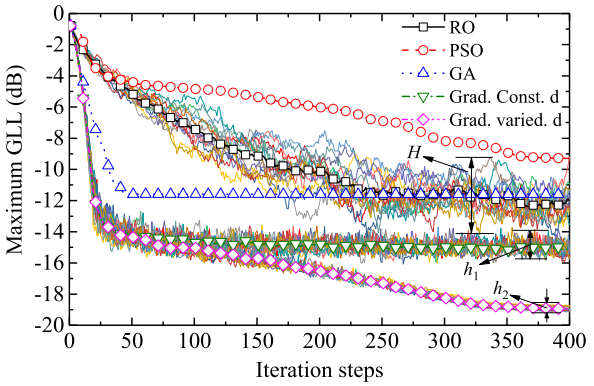

FIGURE 7. Comparison of different algorithms ($d = 0.05\lambda$ for RO, PSO and GA, $a = 4$ for Grad. const. d and Grad. varied d (from 0.05λ to almost 0)).

B. OPTIMIZATION RESULTS AND COMPARISON

Two clusters of curves, corresponding to a constant $d = 0.05\lambda$ and a varied d from 0.05λ to almost 0, are obtained by the proposed gradient algorithm and shown in Fig. 7. By virtue of the d varied as the optimization process, not only early and fast convergence is achieved, but also better convergence results are obtained at the end of optimization.

Besides the algorithm based on the position gradient and sigmoid function, the results obtained with other algorithms including the PSO, GA and random optimization (RO) are also shown in Fig. 7 for the sake of comparison. It is noted that the gradient-sigmoid-based algorithm proposed in this study exhibits faster convergence rate. This is because the displacements of the elements are calculated more reasonably by checking their position gradients. Furthermore, it is precise because the displacement has a reasonable decision basis, which ensures that the gradient-based optimization method possesses better stability when optimizing the same problem many times. More than 15 tests for each algorithm are conducted to verify the stability of the proposed method. Apparently, the fluctuation range H of curve cluster of RO is larger than that of the gradient-sigmoid-based optimization (record as h_1 at a fixed d and h_2 at a dynamic d), and obviously, $h_2 < h_1$, as also shown in Fig. 7. The optimal AF of the 16×16-element array after 1000 iterations is plotted in Fig. 8. The highest GL is effectively suppressed by nearly 20 dB by the proposed algorithm.

C. CAPABILITY VERIFICATION OF SUPER MULTIVARIATE

A planar array with 100 × 100 elements is constructed and optimized by the proposed algorithm. The obtained results are shown in Fig. 9. About 20 thousand variables, the coordinate positions for both axes are controlled at the same time. The non-uniform fast Fourier transform (NuFFT) is used to replace the conventional field superposition and greatly improve the optimization efficiency. Through this way, the pattern calculation can be accelerated. The optimization goal of 32 dB reduction of GLL is achieved. This numerical example is accomplished with a computer (Intel(R) Core (TM) i3-3220 CPU at 3.3 GHz with 16 GB RAM) and

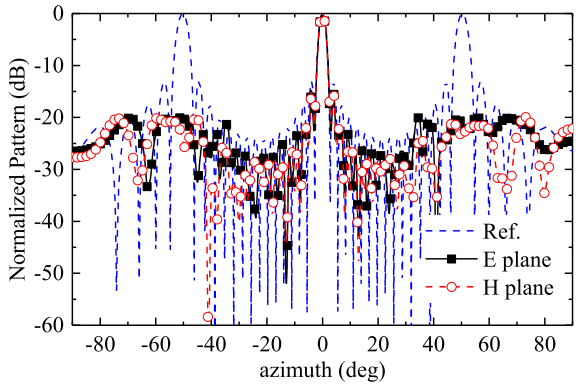

FIGURE 8. Optimal results of AF of 16×16-element array (*E*-plane and *H*-plane).

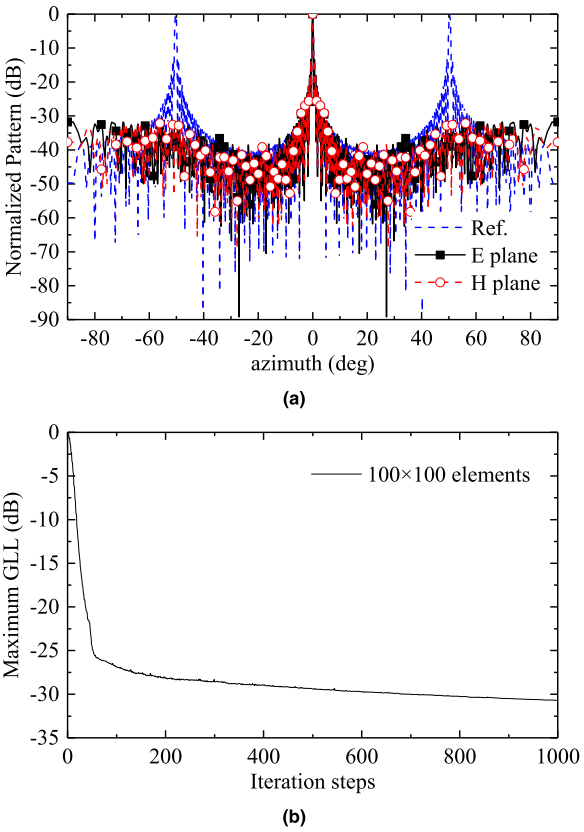

FIGURE 9. Optimal results of AF (E-plane and H-plane) obtained by the proposed algorithm in the case of (a) 100×100-element array (the Ref. curve represents AF of the uniform array with same size), and (b) is the convergence curves.

each iteration generation takes only 6.16 seconds on average by using NuFFT with 4096 × 4096 samples.

IV. GRATING LOBE SUPPRESSION IN SCANNING

In order to present the practicality of the proposed optimization algorithm in real problems, a nested array antenna has been studied and analysis in this section.

A. A LARGE ARRAY MODLE BASED ON SUBARRAYS

A large array antenna based on subarrays is presented and expected to have a feature of low sidelobe, whose sketch map

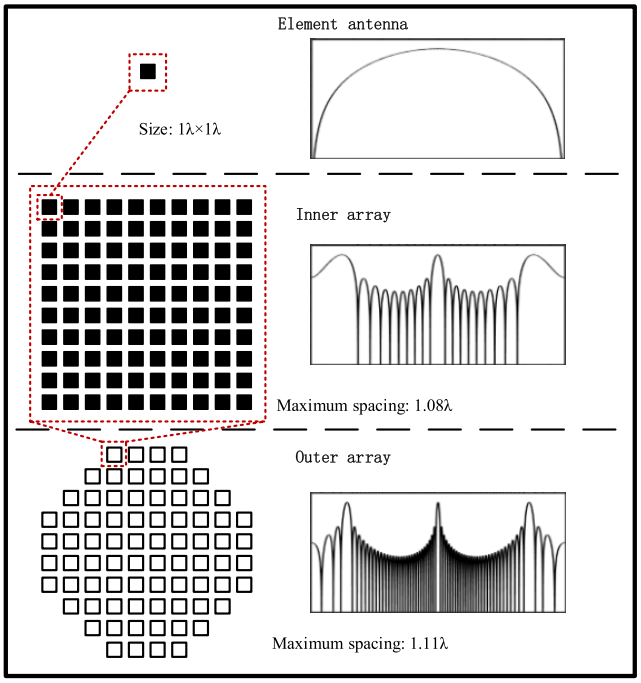

FIGURE 10. Initial layout of the example array in which each hollow square represents a basic subarray with 10×10 antenna elements using solid squares as alternatives. (The patterns in the figure are not the lines based on real data and they are just sketch maps used to exhibit their differences in the three levels of the nested array as example.)

of the initial layout is plotted as Fig. 10. The layout of outer array is set to a rectangular grid of 10×10 subarrays with 6 subarrays at each corner area removed, as shown in the third part of Fig. 10. The maximum size of the whole aperture of this array is limited to 1.11 times of the aperture size of the compact subarray arrangement. In this array, the element antennas in a certain subarray are managed as the distribution of inner array in Fig. 10 with 10×10 units but without element removed. The element spacing in every subarray is set to 1λ, and its maximum limit is set to 1.08λ. Therefore, the final size limit in each direction has a 1.2 times which is determined by 1.08 times 1.11. Because of the element size of 1λ×1λ, the grating lobe appears quickly when the main beam deviates from its boresight direction, so grating lobe suppression is a significant task to be solved by the proposed algorithm.

The aim of low sidelobe is down to -20dB no matter which direction is scanning at least 15 degrees. As well know that the element spacing of array antennas is significantly related to the grating lobe suppression, according to the basic theory of array antenna. In this case of element spacing larger than 1λ, the grating lobes must appear in some normal array antennas when the scanning angle is reaching at 15 degrees. Therefore, the optimization is challenging.

B. STRATEGIES IN THE PROGRESS OF OPTIMIZATION

A basic expectation is that when the array antenna layout is optimized, side lobe suppression can be achieved regardless of elevation or azimuth scanning. It is different from the no-scanning or single-axis-scanning cases because the

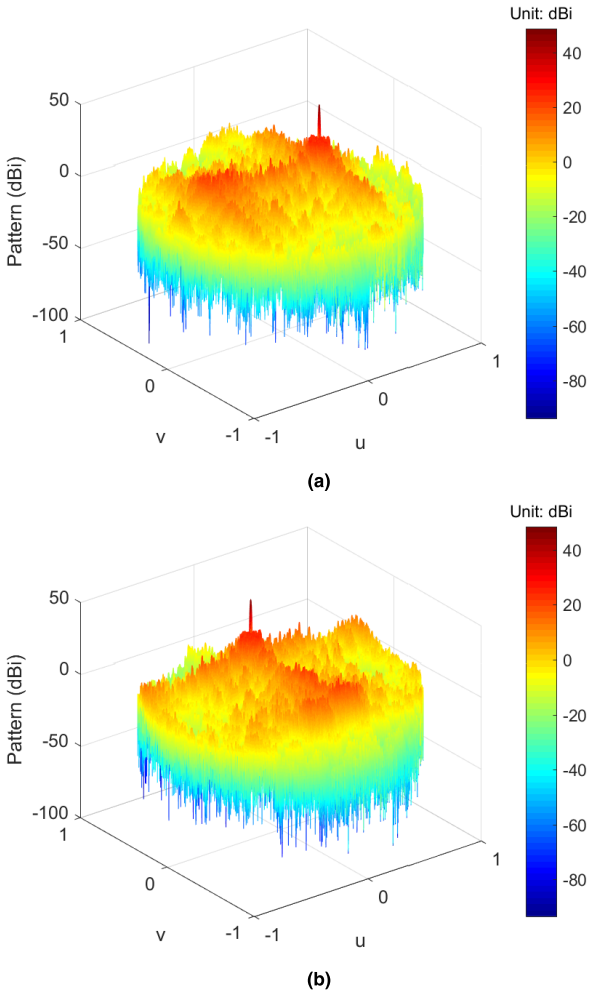

FIGURE 11. Optimized results of 3D pattern of the example large array. (a) Scanned at 20° in the *u*-axis; (b) Scanned at 20° in the *v*-axis.

TABLE 1. Comparison between the optimized and the initial results of the example large array.

	u-axis	*v*-axis
Scan Angle (deg.)	20	20
Initial Gain (dBi)	48.87	48.41
optimized Gain (dBi)	48.87	48.41
Initial SLL (dB)	-6.56	-6.28
optimized SLL (dB)	-22.62	-22.64

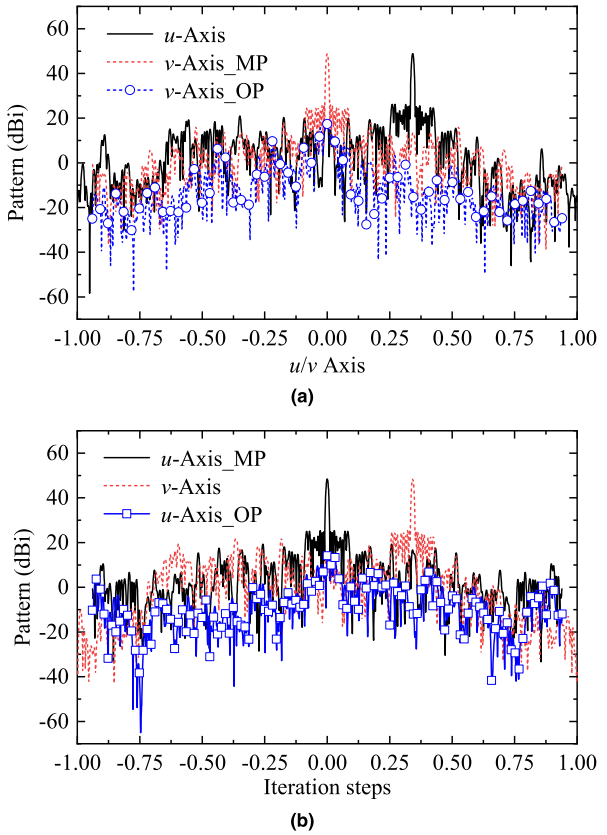

FIGURE 12. Optimized results of 1D pattern of the example large array which are along the *u*-axis or the *v*-axis. The suffix, MP, refers to the main-lobe peak point which means the 1D pattern is going through the main-lobe peak point, and OP refers to the origin point of the coordinate, that means the related 1D pattern is crossing the origin of its coordinate system. Their distributions are paralleling to the *u*-axis or *v*-axis. Line legends without MP or OP indicate that the line passes through these two points. (a) Scanned at 20° in the *u*-axis; (b) Scanned at 20° in the *v*-axis.

algorithm needs to reduce sidelobe level both in two scanning situations at the same time. The basic strategy of optimization is the alternating optimization strategy (AOS), which means the x-axis scanning and the y-axis scanning are set and optimized one by one. In order to avoid the imbalance of the optimizations in two axes, we improve the AOS to be no longer a one-by-one alternative process, but a continuous optimization of a relatively poor direction through the detection of results. Actually, it is an alternating continuous optimization strategy (ACOS). After optimized by using ACOS, the sidelobe levels of the two scanning situations should decrease by an approximate reduction.

To deal with the nested array, the strategy of inner-optimization to outer-optimization (ITO) is carried out. The inner optimization is referring to the subarray optimization by adjusting each single element antenna and the pattern of a subarray is obtained when the iteration of inner optimization is completed. After then, the outer optimization is conducted based on the results of the inner optimization. Because the pattern of inner subarray (or element antenna) is the constituent unit of the pattern calculation of the outer array. The relationship among the element antenna, the inner array and the outer array are actually determined by the layout of whole array as shown in Fig. 10. By using the ITO strategy, we can always maintain the formal distribution of arrays based on subarrays, which is very important for the design procedure and the engineering manufacture of large arrays.

C. OPTIMIZATION RESULTS

To validate the effectiveness of the proposed optimization algorithm, the example of large array in Fig. 10 is took into computation. We use a rectangular horn with its aperture size of $1\lambda \times 1\lambda$ as the element antenna of the subarray which compose the large array. Their active element pattern used

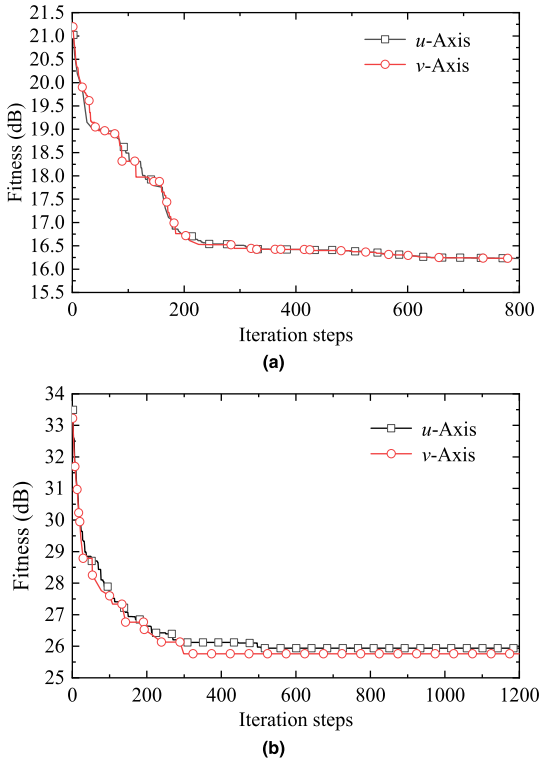

FIGURE 13. Convergence curves of the optimization in the two scanning conditions, respectively. (a) Inner array. (b) Outer array.

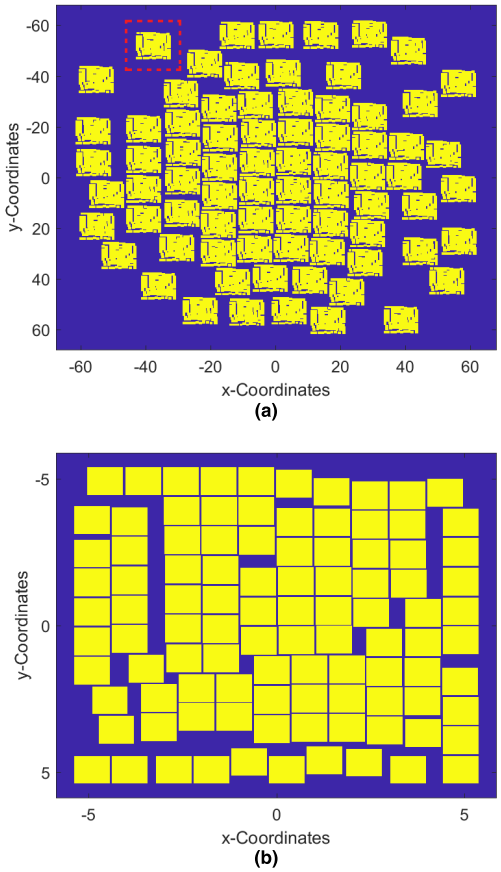

FIGURE 14. Optimized layouts of the example large array. (Unit: λ) (a) The whole array; The part inside the red dashed box is referring to a subarray antenna, whose enlarged map is as shown in (b). (b) Subarray.

for pattern calculation is extracted at the beginning of the optimization and updated at the end of the process of inner-array optimization. That means the AEP of middle element in the subarray is obtained from the optimized subarray, so that some significant parts of the mutual coupling between array elements can be considered. After the two iterative stages of the optimization process, inner-array optimization and outer-array optimization, we finally get the results of 3D patterns which are as shown in the Fig. 11. Some 1D patterns extracted from Fig. 11 are plotted in Fig. 12, which are distributed along the u-axis (x-axis) or v-axis (y-axis) and crossing the main-lobe peak point (MP) or the origin point (OP). It is obvious that the sidelobe level of the 1D patterns are below -20dB when the array is under a working situation of scanning 20 degrees no matter parallel to the u or v axis.

The specific data of the results are listed in Table I. The initial data, including initial Gain and initial SLL, refer to the pattern performance parameters of the array in the case of rectangular grid layout as designed in Fig. 10. The initial array is without any random element displacement which has an element spacing 1.08λ and a subarray spacing 11.988λ, both mentioned at the second paragraph of the section IV in this paper. By comparing with the initial data, the optimized results can prove the effectiveness of the optimization algorithm we proposed. In particular, the SLLs, i.e. the difference of the peak gain and the maximum sidelobe gain, are reduced by 16.06dB and 16.36dB through optimization respectively in the two axes. At the meanwhile, the peak gains are not affected a lot.

The convergence curves of the two iterative stages in the optimization process, referring to the optimization of the inner array and that of the outer array, can further confirm the reliability of our proposed algorithm, as shown in Fig. 13. During the optimization process of the inner array, the final maximum gain inside all the sidelobe region of the subarray is suppressed down to approximately 16.24dB. After the outer iteration, the optimized sidelobe gain is reduced by nearly 7.5dB, and down to 26.24dB and 25.76dB in the two axes, respectively. They are consistent with the data in the Table 1. Here in Fig. 13, the first iteration results are calculated in the situation of using a non-uniform array antenna formed by summing the initial grid array with regular-distributed layout and a random data array of displacement, rather than directly using the initial one as shown in Fig. 10. The random displacement array can make the initial phase distribution more random and facilitate the optimization process, and it can be generated by a random function with scale constraints.

To demonstrate that the obtained results satisfy the range constraints and the overlapping constraints, a real layout map of whole array is plotted in Fig. 14(a). The lighted part of blocks in the red dashed box represents a subarray of the example array. Through observation, there is no

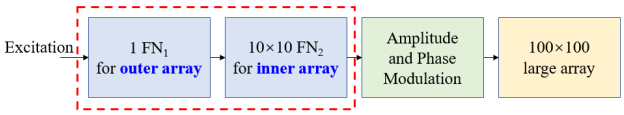

FIGURE 15. The cascade diagram of the feed network (FN) of the 10000-element array. Only two types of FNs are needed for the large array (in the dashed box). Both of FN_1 and FN_2 have one input port and 10×10 output ports. The complete FN consists of one FN_1 and 10×10 FN_2 by using cascade mode, to match the outer and inner arrays, respectively.

obvious overlaps in the map which proves that the subarrays are separated from each other. As to the inner layout of the subarray, an enlarged map is plotted in Fig. 14(b). Similarly, the composed elements have no overlap parts to each other. On the other hand, the aperture of arbitrary subarray and the whole array are constrained inside an area of $10.8\lambda\times10.8\lambda$ and $120\lambda\times120\lambda$, respectively. In a word, the optimization process using the proposed algorithm strictly complies with the expected constraints and meets the requirements.

By the way, the feed network (FN) of the example array can be designed as two levels (FN_1 and FN_2) to match the outer array with 10×10 subarrays and the inner array with 10×10 elements, respectively, as shown in Fig. 15. That means each output port of the outer FN_1 connects an inner FN_2 which also has one input port and 10×10 output ports. This convenient approach benefits from that all subarray layouts are the same. Compared to the Completely random array, the design complexity of feed network is greatly reduced.

V. CONCLUSION

In this paper, an effective optimization algorithm based on position gradient and sigmoid function has been proposed for non-uniform large-spacing array. Through the proposed algorithm, GLS optimization for especially large-scale array antennas, which are difficult for the conventional global optimization algorithms to deal with the overwhelming variables, become convenient and efficient. The sigmoid function is used to control and optimize the iterative process. Its effectiveness is verified by the result of the 16×16-element array. A huge array with 10000 elements, up to 20 thousand position variables, has been optimized to demonstrate the efficiency of the proposed algorithm for grating lobe suppression. The results of another large array antenna based on subarrays has met the expectation of a low SLL of -20dB, which proves the effectiveness of our proposed algorithm in large practical layouts.

REFERENCES

[1] C. I. Coman, I. E. Lager, and L. P. Ligthart, "The design of shared aperture antennas consisting of differently sized elements," *IEEE Trans. Antennas Propag.*, vol. 54, no. 2, pp. 376–383, Feb. 2006.

[2] G. Han, B. Du, W. Wu, and B. Yang, "A novel hybrid phased array antenna for satellite communication on-the-move in Ku-band," *IEEE Trans. Antennas Propag.*, vol. 63, no. 4, pp. 1375–1383, Apr. 2015.

[3] K. F. Warnick, R. Maaskant, M. V. Ivashina, D. B. Davidson, and B. D. Jeffs, "High-sensitivity phased array receivers for radio astronomy," *Proc. IEEE*, vol. 104, no. 3, pp. 607–622, Mar. 2016.

[4] S. J. Wijnholds, W. A. van Cappellen, J. G. B. de Vaate, and A. van Ardenne, "Antenna applications corner: Phased-array antenna system development for radioastronomy applications," *IEEE Antennas Propag. Mag.*, vol. 55, no. 6, pp. 293–308, Dec. 2013.

[5] Q. Cheng, A. Alomainy, and Y. Hao, "Compressive millimeter-wave phased array imaging," *IEEE Access*, vol. 4, pp. 9580–9588, 2016.

[6] Y. V. Krivosheev, A. V. Shishlov, and V. V. Denisenko, "Grating lobe suppression in aperiodic phased array antennas composed of periodic subarrays with large element spacing," *IEEE Trans. Antennas Propag.*, vol. 57, no. 1, pp. 76–85, Feb. 2015.

[7] H. Wang, D.-G. Fang, and Y. L. Chow, "Grating lobe reduction in a phased array of limited scanning," *IEEE Trans. Antennas Propag.*, vol. 56, no. 6, pp. 1581–1586, Jun. 2008.

[8] P. J. Bevelacqua and C. A. Balanis, "Geometry and weight optimization for minimizing sidelobes in wideband planar arrays," *IEEE Trans. Antennas Propag.*, vol. 57, no. 4, pp. 1285–1289, Apr. 2009.

[9] L. Poli, P. Rocca, L. Manica, and A. Massa, "Pattern synthesis in time-modulated linear arrays through pulse shifting," *IET Microw., Antennas Propag.*, vol. 4, no. 9, pp. 1157–1164, Sep. 2010.

[10] R. L. Haupt, "Optimized weighting of uniform subarrays of unequal sizes," *IEEE Trans. Antennas Propag.*, vol. 55, no. 4, pp. 1207–1210, Apr. 2007.

[11] H. Orazi, H. Soleimani, and R. Azadkhah, "Synthesis of linearly polarised patterns of conical arrays by the method of least square," *IET Microw., Antennas Propag.*, vol. 9, no. 2, pp. 185–191, Jan. 2015.

[12] Y. Liu, X. Huang, K. D. Xu, Z. Song, S. Yang, and Q. H. Liu, "Pattern synthesis of unequally spaced linear arrays including mutual coupling using iterative FFT via virtual active element pattern expansion," *IEEE Trans. Antennas Propag.*, vol. 65, no. 8, pp. 3950–3958, Aug. 2017.

[13] D. Dai, M. Yao, H. Ma, W. Jin, and F. Zhang, "An effective approach for the synthesis of uniformly excited large linear sparse array," *IEEE Antennas Wireless Propag. Lett.*, vol. 17, no. 3, pp. 377–380, Mar. 2018.

[14] M. E. Yigit and T. Giinel, "Pattern Synthesis of Linear Antenna Array via a New Hybrid Taguchi- Genetic-Particle Swarm Optimization Algorithm," in *Proc. 18th Medit. Microw. Symp. (MMS)*, Istanbul, Turkey, Oct./Nov. 2018, pp. 17–21.

[15] D. G. Kurup, M. Himdi, and A. Rydberg, "Synthesis of uniform amplitude unequally spaced antenna arrays using the differential evolution algorithm," *IEEE Trans. Antennas Propag. Mag.*, vol. 51, no. 9, pp. 2210–2217, Sep. 2003.

[16] P. Chakravorty and D. Mandal, "Grating lobe suppression with discrete dipole element antenna arrays," *IEEE Antennas Wireless Propag. Lett.*, vol. 15, pp. 1234–1237, 2015.

[17] W. P. M. N. Keizer, "Large planar array thinning using iterative FFT techniques," *IEEE Trans. Antennas Propag.*, vol. 57, no. 10, pp. 3359–3362, Oct. 2009.

[18] F. Yang, S. Yang, Y. Chen, S. Qu, and J. Hu, "Convex optimization of pencil beams through large-scale 4-D antenna arrays," *IEEE Trans. Antennas Propag.*, vol. 66, no. 7, pp. 3453–3462, Jul. 2018.

[19] P. Cao, J. S. Thompson, and H. Haas, "Constant modulus shaped beam synthesis via convex relaxation," *IEEE Antennas Wireless Propag. Lett.*, vol. 16, pp. 617–620, 2016.

[20] A. Benini, E. Martini, S. Monni, M. C. Viganò, F. Silvestri, and E. Gandini "Phase-gradient meta-dome for increasing grating-lobe-free scan range in phased arrays," *IEEE Trans. Antennas Propag.*, vol. 66, no. 8, pp. 3973–3982, Aug. 2018.

[21] C. Lu, W. Sheng, Y. Han, and X. Ma, "Phase-only pattern synthesis based on gradient-descent optimization," *J. Syst. Eng. Electron.*, vol. 27, no. 2, pp. 297–307, Apr. 2016.

[22] C.-H. Tsai, Y.-T. Chih, W. H. Wong, and C.-Y. Lee, "A hardware-efficient sigmoid function with adjustable precision for a neural network system," *IEEE Trans. Circuits Syst. II, Exp. Briefs*, vol. 62, no. 11, pp. 1073–1077, Nov. 2015.

[23] R. Shrestha, S. K. Mohammed, M. M. Hasan, X. Zhang, and K. A. Wahid, "Automated adaptive brightness in wireless capsule endoscopy using image segmentation and sigmoid function," *IEEE Trans. Biomed. circuits Syst.*, vol. 10, no. 4, pp. 884–892, Aug. 2016.

XIAOMIN XU received the B.E. degree in electronic information science and technology from Southwest Jiaotong University, Chengdu, China, in 2013, where he is currently pursuing the Ph.D. degree in electromagnetic field and microwave technology with the School of Physical Science and Technology.

His current research interests include base-station antenna design, antenna array technology with electrically large property, synthesis technology of large array antenna, and electromagnetic optimization algorithm.

CHENG LIAO received the B.S. and M.S. degrees in optics and the Ph.D. degree in electromagnetic field and microwave technology from the University of Electronic Science and Technology of China (UESTC), Chengdu, China, in 1986, 1989, and 1995, respectively.

He is currently a Professor and the Director of the Institute of Electromagnetic Field and Microwave Technology, Southwest Jiaotong University, Chengdu. His research interests include antennas and propagation, computational electromagnetics, electromagnetic scattering, and inverse scattering.

LIANG ZHOU received the B.S. degree from the University of Electronic Science and Technology of China (UESTC), Chengdu, China, and the Ph.D. degree in electromagnetic field and microwave technology from the School of Physical Science and Technology, Southwest Jiaotong University, Chengdu, in 2012 and 2018, respectively.

He is currently with the 724 Research Institute, China Shipbuilding Industry Corporation (CSIC), Nanjing, China, where he conducts research on computational electromagnetics and electromagnetic wave propagation.

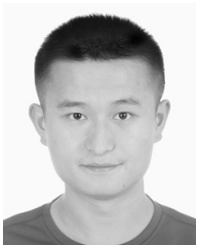

FAN PENG received the B.E. degree in electronic information science and technology from the Chengdu University of Information and Technology, China, in 2016. He is currently pursuing the Ph.D. degree in philosophy with the School of Physical Science and Technology, Southwest Jiaotong University, China.

His research interests include array synthesis technology with convex optimization and electromagnetic optimization algorithm.